Molecular Cell
Article

Diphosphothreonine-Specific Interaction between an SQ/TQ Cluster and an FHA Domain in the Rad53-Dun1 Kinase Cascade

Hyun Lee,[1,3,10] Chunhua Yuan,[4,10] Andrew Hammet,[7] Anjali Mahajan,[3] Eric S.-W. Chen,[1,9] Ming-Ru Wu,[1,9] Mei-I Su,[1] Jörg Heierhorst,[7,8,*] and Ming-Daw Tsai[1,2,3,4,5,6,9,*]
[1]Genomics Research Center
[2]Institute of Biological Chemistry
Academia Sinica, Taipei 115, Taiwan
[3]Biophysics Program
[4]Campus Chemical Instrument Center
[5]Department of Chemistry
[6]Department of Biochemistry
Ohio State University, Columbus, OH 43210, USA
[7]St. Vincent's Institute of Medical Research
[8]Department of Medicine
St. Vincent's Health, The University of Melbourne, Fitzroy, Victoria 3065, Australia
[9]Institute of Biochemical Sciences, National Taiwan University, Taipei 10617, Taiwan
[10]These authors contributed equally to this work
*Correspondence: mdtsai@gate.sinica.edu.tw (M.-D.T.), jheierhorst@svi.edu.au (J.H.)
DOI 10.1016/j.molcel.2008.05.013

SUMMARY

Forkhead-associated (FHA) domains recognize phosphothreonines, and SQ/TQ cluster domains (SCDs) contain concentrated phosphorylation sites for ATM/ATR-like DNA-damage-response kinases. The Rad53-SCD1 has dual functions in regulating the activation of the Rad53-Dun1 checkpoint kinase cascade but with unknown molecular mechanisms. Here we present structural, biochemical, and genetic evidence that Dun1-FHA possesses an unprecedented diphosphothreonine-binding specificity. The Dun1-FHA has >100-fold increased affinity for diphosphorylated relative to monophosphorylated Rad53-SCD1 due to the presence of two separate phosphothreonine-binding pockets. In vivo, any single threonine of Rad53-SCD1 is sufficient for Rad53 activation and *RAD53*-dependent survival of DNA damage, but two adjacent phosphothreonines in the Rad53-SCD1 and two phosphothreonine-binding sites in the Dun1-FHA are necessary for Dun1 activation and *DUN1*-dependent transcriptional responses to DNA damage. The results uncover a phospho-counting mechanism that regulates the specificity of SCD, and provide mechanistic insight into a role of multisite phosphorylation in DNA-damage signaling.

INTRODUCTION

Posttranslational protein modifications, including ubiquitination and phosphorylation, play crucial roles in the regulation of cellular DNA-damage responses (Kim et al., 2007; Kolas et al., 2007). ATM/ATR-like kinases act upstream in the DNA-damage response and phosphorylate hundreds of substrates preferentially on SQ/TQ motifs (Matsuoka et al., 2007; Stokes et al., 2007) that often occur concentrated in characteristic SCDs (Traven and Heierhorst, 2005). The importance of protein phosphorylation is also reflected in the prevalence of modular phosphopeptide-binding domains among DNA-damage-response proteins, including BRCT domains that can bind phosphoserine (pSer) or phosphothreonine (pThr) (Manke et al., 2003), and the pThr-specific FHA domains (Durocher et al., 2000; Li et al., 2002, 2004; Liao et al., 2000; Sun et al., 1998; Tanaka et al., 2001).

Rad53 and Dun1 are structurally and functionally related kinases (Figure 1A) that play important roles in the DNA-damage response in *Saccharomyces cerevisiae* (Bashkirov et al., 2003; Durocher and Jackson, 2002; Lee et al., 2003b; Traven and Heierhorst, 2005). They are part of a central checkpoint kinase cascade, where the ATM/ATR-like kinases Mec1/Tel1 first activate Rad53, which in turn activates Dun1 (Sanchez et al., 1996). This cascade regulates several DNA-damage-response pathways, such as the G2/M cell-cycle arrest checkpoint (Gardner et al., 1999), posttranslational regulation of dNTP levels (Zhao and Rothstein, 2002), and transcriptional (Hammet et al., 2000; Matsuoka et al., 1998) and posttranscriptional (Hammet et al., 2002) regulation of gene expression. However, the two kinases can also act independently of each other in other parts of the DNA-damage response: for example, Rad53, but not Dun1, is required to stabilize stalled replication forks to allow completion of S phase (Lopes et al., 2001; Tercero and Diffley, 2001), whereas Dun1 appears to be more important than Rad53 to prevent gross chromosomal rearrangements (Myung et al., 2001).

Rad53 and Dun1 are characterized by the presence of FHA domains that are important for their activation in response to DNA damage, and Rad53 also contains two SCDs of concentrated

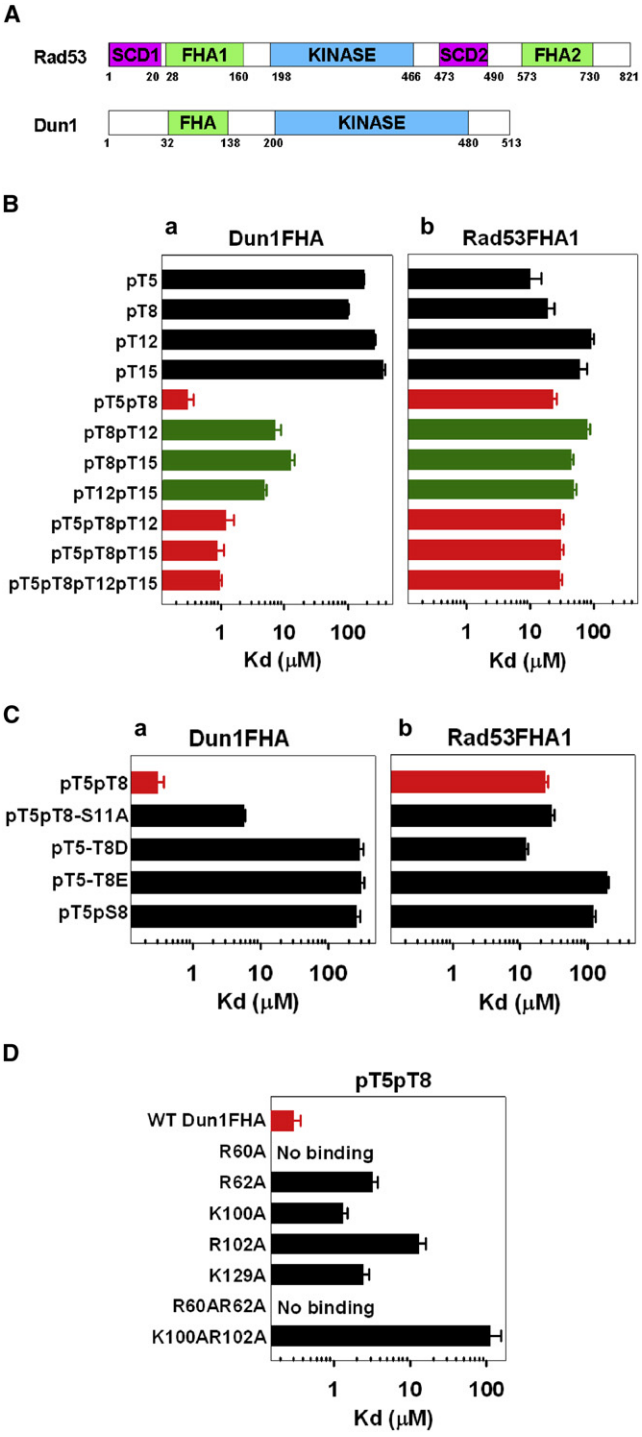

Figure 1. Biochemical Evidence for SCD1 Double-Phosphorylation Requirement of the Dun1-FHA

(A) Diagram of yeast Dun1 and Rad53. They share 18.8% of sequence identity and 29.4% similarity in their entire sequences (35.5% and 53%, respectively, within the kinase domain) (Bashkirov et al., 2003).

(B) SPR data (K_D) of phosphopeptides for Dun1-FHA (Ba) and Rad53-FHA1 (Bb).

(C) Comparison of K_D values between pT5pT8 and its analogs and between WT Dun1-FHA (Ca) and Rad53-FHA1 (Cb). Analyses of the Dun1-FHA data are described in the text. As expected, Rad53-FHA1 binds these analogs with affinities in the same order of magnitude as those shown in Figure 1Bb, but pT5-T8D has the lowest K_D among the analogs.

(D) The K_D values between Dun1-FHA mutants and pT5pT8 in comparison with WT Dun1-FHA. The procedures for K_D measurements by SPR have been described previously (Durocher et al., 2000; Liao et al., 2000). All data were fit to a single rectangular hyperbolic curve to calculate the K_D, and the error bars represent standard errors from two to four independent experiments or fitting curves. "No binding" means K_D > 100 μM.

Mec1/Tel1 phosphorylation sites (Bashkirov et al., 2003; Hammet et al., 2000; Lee et al., 2003b; Pike et al., 2003; Sweeney et al., 2005). Interestingly, the N-terminal Rad53-SCD1 seems to have two separate functions during Rad53 and Dun1 activation (Bashkirov et al., 2003; Lee et al., 2003b). The Rad53-SCD1 contains four threonine residues, and a recent phosphoprotein analysis study found that each of these residues is in principle phosphorylatable (Smolka et al., 2005). Simultaneous substitution of the four threonines by alanine (Rad53-SCD1-4AQ) dramatically impairs Rad53 activation in response to DNA damage, which can be fully restored by add-back of any single threonine (Lee et al., 2003b). The phosphorylated Rad53-SCD1 can also be bound by the Dun1-FHA domain to promote phosphorylation-dependent activation of Dun1 by Rad53 (Bashkirov et al., 2003; Lee et al., 2003b). However, in contrast to Rad53 activation, restoration of any single threonine in Rad53-SCD1-4AQ is insufficient for Dun1 activation (Lee et al., 2003b).

It is unresolved whether Dun1-FHA ligand specificity simply requires additional (unphosphorylated) threonine residues near the pThr-binding site or multisite phosphorylation and, if so, on how many sites and more specifically which sites. Moreover, the dual role of the Rad53-SCD1 in Rad53 and Dun1 activation represents a puzzling question for the mechanism of how a single phosphorylation site cluster can regulate the sequential activation of two separate kinases in a temporally ordered manner. To resolve these questions, we have here combined detailed biochemical, structural, and genetic analyses that reveal an unprecedented double-threonine-specific binding mode of the Dun1-FHA domain that is required for Dun1 activation and *DUN1* functions in vivo.

RESULTS

The Dun1-FHA Domain Preferentially Binds to Multiphosphothreonine-Containing Rad53-SCD1 Peptides In Vitro

In order to test if multisite phosphorylation of the Rad53-SCD1 could be required for Dun1 activation, we systematically examined binding affinity between variously phosphorylated peptides derived from Rad53-SCD1 (^{1}MENIT^{5}QPT^{8}QQST^{12}QAT^{15}QRFLIE^{21}) and the recombinant Dun1-FHA domain (Hammet et al., 2000) by surface plasmon resonance (SPR). The peptides are named hereafter by their phosphorylated residues; for example, pT5pT8 designates the SCD1 peptide with phosphorylation at both Thr5 and Thr8. No binding was observed between the Dun1-FHA and the unphosphorylated SCD1 peptide. The dissociation equilibrium constant (K_D) values of phosphorylated peptides are plotted in Figure 1Ba, which shows three categories

of binding affinities: (1) K_D values in the order of 100 μM were observed for the four monophosphorylated peptides (black bars); (2) remarkably, ~100-fold lower K_D values of 0.3–1.2 μM were observed for the peptides with both Thr5 and Thr8 phosphorylated, including peptides with phosphorylation at additional sites (red bars); (3) peptides with two or more pThr residues, but lacking simultaneous phosphorylation on Thr5 and Thr8, displayed intermediate K_D values in the order of 10 μM (green bars).

For comparison, Rad53-FHA1 bound all single- and multiple-phosphorylated peptides with similar but modest affinity (K_D = 10–90 μM), with pT5, pT8, and pT5pT8 having the lowest K_D (10–20 μM) (Figure 1Bb). Furthermore, none of the SCD1 phosphopeptides tested (pT5, pT8, pT12, pT15, pT5pT8, pT12pT15, and pT5pT8pT12pT15) showed detectable binding affinity (K_D ~100 μM) to the FHA2 domain of Rad53 in SPR experiments (data not shown). Unphosphorylated SCD1 peptide could not bind to any of the three FHA domains tested above. Taken together, these results suggest that diphosphorylated SCD1, particularly the one involving pThr5 and pThr8, may be the natural ligand for Dun1-FHA and that SCD1 monophosphorylation may be sufficient for Rad53-FHA1 binding.

NMR Structural Analysis of the Dun1-FHA Domain

Nuclear magnetic resonance (NMR) was then used to examine the structural basis of the seemingly unique ligand specificity of the Dun1-FHA domain. First we solved the previously unknown structure of the Dun1-FHA (Figure 2A and see Table S1 available online). Its core architecture of a twisted β sandwich formed by 11 β strands is overall similar to all other solved FHA domains, including Rad53-FHA1 (Lee et al., 2003a; Li et al., 2004; Liao et al., 1999, 2000; Stavridi et al., 2002), despite considerable sequence divergence (Figure 2B). As shown in Figure 2C, major structural differences between Dun1-FHA and Rad53-FHA1 are found in the loops—Rad53-FHA1 has a short α helix connecting β2 and β3 and another one immediately following β11; Rad53-FHA1 also has a longer β10/β11 loop, while Dun1-FHA has an extended β5/β6 interaction.

Identification of a Second pThr-Binding Site in the Dun1-FHA Domain

Two-dimensional (2D) ^{1}H-^{15}N heteronuclear single quantum coherence (HSQC) spectra were then recorded upon peptide titration. These HSQC analyses independently confirmed the SPR analyses, that pThr5-pThr8 double phosphorylation is required and sufficient for the tightest binding of SCD1 to Dun1-FHA and causes most extensive chemical shift perturbations (Figure 3A), virtually identical to spectra of the pT5pT8pT12pT15 peptide (data not shown). Interestingly, separate addition of the monophosphorylated peptides pT5 and pT8 caused independent effects on the relevant pThr-binding residues (e.g., the backbone amides of Arg62 and Thr75 and the three NH^{ε}/Arg resonances in Figure S2), suggesting the existence of two distinct pThr-binding sites in Dun1-FHA.

A ten-residue pT5pT8 peptide, ^{3}NI(pT)QP(pT)QQST^{12}, was then used to determine the structure of the complex with Dun1-FHA. Forty-two intermolecular NOEs were assigned in three-dimensional (3D) $^{13}C/^{15}N$-filtered (*f*1), ^{13}C-edited (*f*3) NOESY, and 3D ^{15}N-edited NOESY, most of which are to the methyl groups of the pThr5 and pThr8 and the side-chain protons of Ser11. The structure of the complex is shown in Figure 4A and

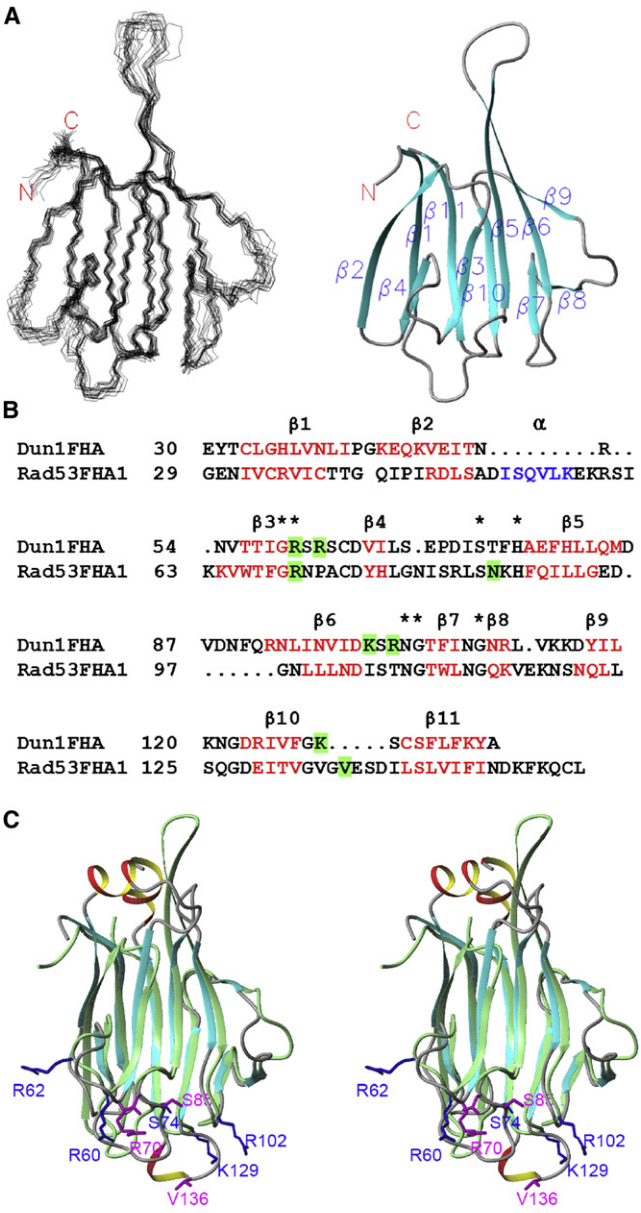

Figure 2. Structural Comparison of Dun1-FHA and Rad53-FHA1

(A) Structure of free Dun1-FHA (19–159). Only the structured part (residues Glu30-Ala138) is shown.

(B) Structure-based sequence alignment between Dun1-FHA and Rad53-FHA1. The residues in β strands and helical conformations are highlighted in red and blue, respectively. Conserved residues among FHA domains are indicated by asterisks. The key residues for phosphopeptide binding are highlighted in green.

(C) Stereo views of the overlay of the ribbon diagrams of free Dun1-FHA (pale green) and free Rad53-FHA1 (cyan). Some key residues for the peptide binding are highlighted: Arg60, Arg62, Ser74, Lys100, Arg102, and Lys129 of Dun1-FHA (in blue) and Arg70, Ser85, and Val136 of Rad53-FHA1 (in magenta).

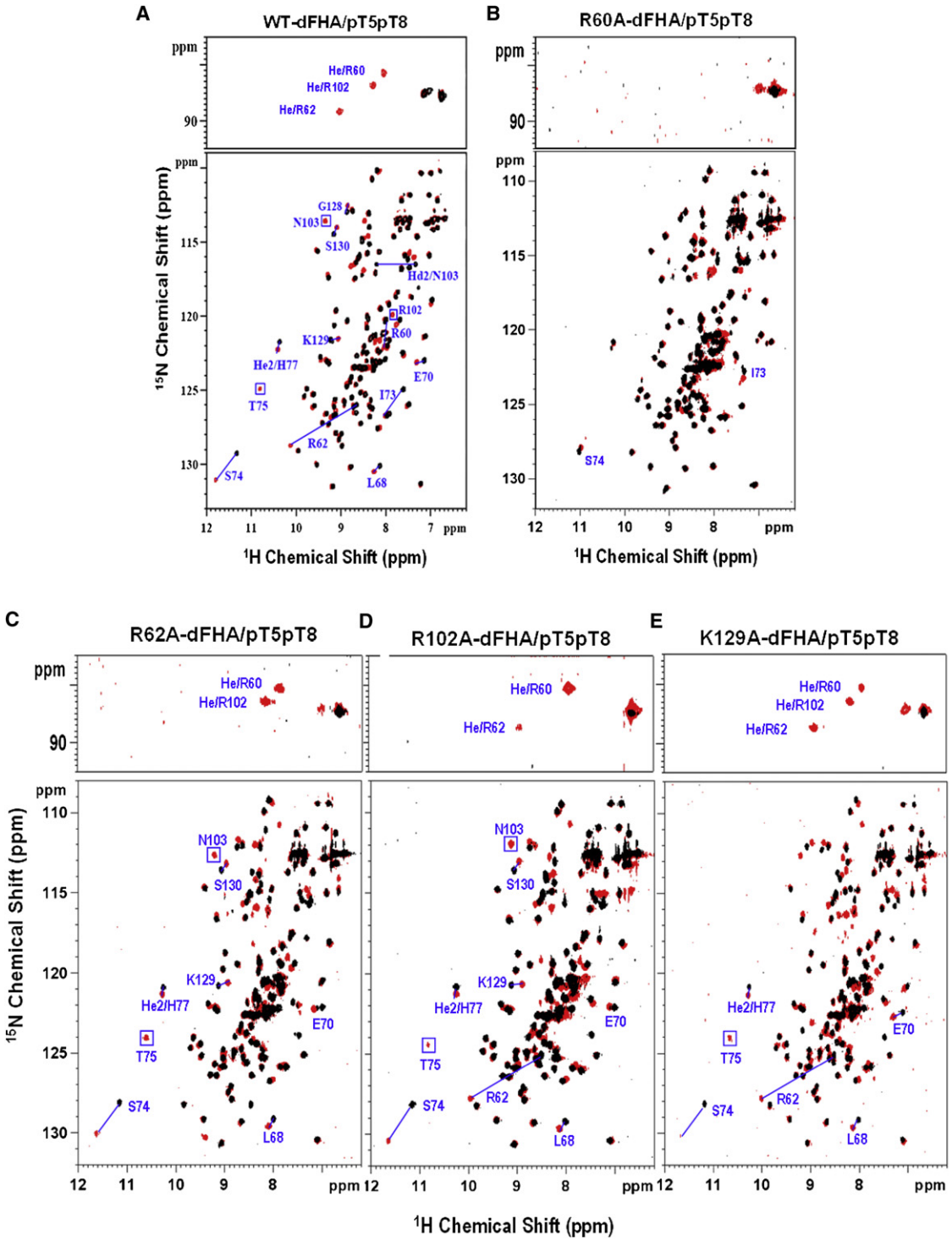

Figure 3. Chemical Shift Changes of WT and Some Mutants of Dun1-FHA upon Binding to the pT5pT8 Peptide Monitored by 2D ^{1}H-^{15}N HSQC

Black and red spectra represent free and complex forms, respectively. Several important residues that exhibit large chemical shift perturbations (e.g., Arg62, Ser74, Lys129, and Ser130) or reappear in the complex form (Thr75, Arg102, and Asn103, boxed) are labeled. The top panel shows the changes in NH^{ε}/Arg. (A) WT Dun1-FHA. (B) R60A, which shows little change upon binding, consistent with the lack of binding (K_D > 100 μM) conclusion from SPR analyses. (C–E) R62A, R102A, and K129A, respectively. The chemical shift changes upon binding follow the same pattern as WT. The data taken together with other results led to the NH^{ε} resonance assignments of R60, R62, and R102 as labeled and further support the "independent and additive role" of these Arg residues.

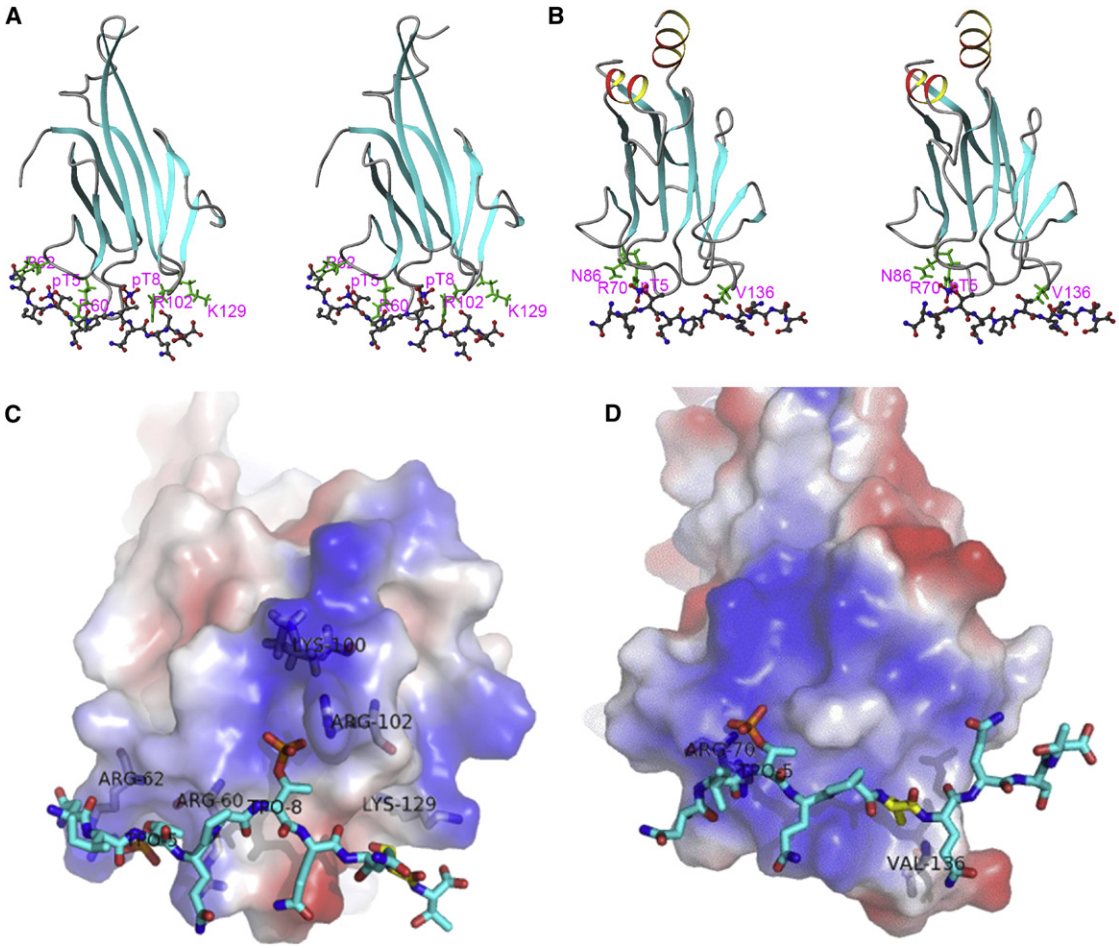

Figure 4. Comparison of Dun1-FHA/Rad53-SCD1 and Rad53-FHA1/Rad53-SCD1 Complexes

(A) Stereo view (side-by-side mode) of the structure of the Dun1-FHA/pT5pT8 complex, as explained in the text.

(B) Structure of the Rad53-FHA1/pT5 complex, which is very similar to the reported Rad53-FHA1/Mdt1-pT305 complex (Mahajan et al., 2005). In both (A) and (B), the peptide is shown in ball and stick (heavy atom only) and the FHA domain in ribbon diagram.

(C and D), Close-up views and charge distributions of the binding surface of structures shown in (A) and (B), respectively. Positive, negative, and neutral potentials are blue, red, and white, respectively.

Figure S1A and the structural data are summarized in Table S1. By analogous procedures, the structure of the complex between the singly phosphorylated peptide pT5, ^{3}NI(pT)QPTQQST^{12}, and Rad53-FHA1 was also solved, and the results are provided in Figure 4B, Figure S1B, and Table S2.

Comparison of the structures of the two complexes reveals a similar binding region involving conserved (Arg60 and Ser74) and nonconserved (e.g., Thr75) residues in β3/β4, β4/β5, β6/β7, and β10/β11 loops/turns. However, significant differences exist behind this similarity by inspection of the structures of the complexes. First, Dun1-FHA has two pThr-binding sites: Arg60 and Arg62 interact with the first pThr at position 5, whereas Arg102 and possibly Lys100 (farther away but supported by mutagenesis results, see below) interact with the second pThr at position 8 (Figure 4C). Second, β3/β4 and β4/β5 loops, interacting largely with pThr5 and pThr8, respectively, make comparatively more extensive contact to accommodate a longer peptide motif. It is noteworthy that Arg60 (in β3/β4) and Ser74 (in β4/β5)—whose counterparts in other complexes interact with the same phosphate group—appear to interact with different pThr residues of SCD1. It appears that some of the residues involved in the "canonical" pThr site of the FHA domain are split to form the two pThr-binding sites in Dun1, each assisted by additional, nonconserved residues. Lastly, Ser11 of the peptide makes considerable contribution to the binding, evidenced by its strong NOE to Lys129 in β10/β11 loop (Figure S3) and large chemical shift perturbations of residues 128–132 (Figure 3A). Taken together, the specificity for diphosphorylated SCD1 peptide appears to be conferred by three key determinants that constitute an optimal ligand motif pTXXpTXXS. To a good approximation, these three interactions are stabilized by the pair of Arg60 and Arg62 (for pThr5), Arg102 and Lys100 (for pThr8), and Lys129 (for Ser11) in the Dun1-FHA domain, respectively (Figures 4A and 4C). In subsequent discussions, the sites binding pT5 and pT8 are referred to as the first and the second pT sites, respectively, of Dun1 FHA.

Both Dun1-FHA Domain Phosphopeptide-Binding Sites Are Highly pThr Specific

We then used additional phosphopeptides to biochemically confirm the binding features revealed in the Dun1-FHA/pT5pT8 complex structure. The results of peptide analogs (Figure 1Ca) show that the K_D increased from 0.3 μM for pT5pT8 to 5.6 μM for pT5pT8-S11A, supporting the involvement of Ser11 in binding. Most significantly, the K_D of pT5-T8D, pT5-T8E, and pT5pS8 all increased to the same order of magnitude as that of single phosphorylated peptides (pT5, pT8, pT12, and pT15), indicating that the second phosphate group cannot simply be replaced by a negatively charged amino acid side chain (Asp or Glu) and that the second phosphopeptide-binding pocket is also highly pThr specific and does not bind pSer, just like the pThr-binding sites in all other FHA domains studied. Taken together, the results indicate a truly unique diphosphate-specific binding mode of Dun1-FHA, which is not simply a variation of the pTXXD preference of Rad53-FHA1.

Dun1-FHA mutants were further used to test the binding features. The results shown in Figure 1D quantitatively confirm the contributions of specific residues in the two separate pThr-binding sites: (1) as expected, the conserved Arg60 is the key residue in the first pThr-binding site, since R60A abolishes binding while R62A weakens the binding only by 10-fold; (2) likewise, Arg102 is the primary residue interacting with pThr8 in the second pThr-binding site as R102A increased the K_D by 43-fold; Lys100 also likely contributes to binding, since the K_D increased by 4- to 5-fold for K100A, and more importantly K100A showed a strong synergistic effect with R102A; (3) the role of Lys129 suggested by the structural work is supported by an 8-fold increase in K_D for the K129A mutant. In addition to the binding assays by SPR, the structural properties of the mutants in the free and complexed forms were analyzed by 2D ^{1}H-^{15}N HSQC, and their results and interpretations are described in Figures 3B–3E.

Dual Rad53-SCD1 Phosphorylation Sites and Dual pThr-Binding Sites of Dun1-FHA Are Required for Dun1 Activation In Vivo

To provide supporting biological evidence for the biochemical and structural data presented above, we generated four new *rad53* alleles by site-directed mutagenesis of the chromosomal *RAD53* locus: *rad53-4AQ* (all four threonine-to-alanine), *rad53-T5-3AQ*, *rad53-T8-3AQ*, and *rad53-T5-T8-2AQ* (where Thr5, Thr8, or both, respectively, were "added back"). Rad53 and Dun1 levels and characteristic phosphorylation-dependent mobility shifts after methyl methanesulfonate (MMS) treatment were monitored by western blotting (Figure 5A). All mutants expressed Rad53 at levels comparable to wild-type (WT), and the observed DNA-damage-induced shifts are similar to plasmid-based complementation assays reported previously (Lee et al., 2003b). Next we measured Rad53 and Dun1 kinase activity in these strains. As shown in Figure 5B, the DNA-damage-induced (auto-)kinase activity of Rad53 was dramatically reduced in the *rad53-4AQ* strain but partially restored in *rad53-T5-3AQ* and *rad53-T8-3AQ* and not further enhanced in *rad53-T5-T8-2AQ*. In contrast, immunoprecipitation (IP) kinase activity of Dun1 toward a synthetic peptide under the same conditions was only marginally improved in *rad53-T5-3AQ* and *rad53-T8-3AQ* but fully restored in *rad53-T5-T8-2AQ* (Figure 5C). Furthermore, in contrast to the single-Thr add-back alleles, *rad53-T5-T8-2AQ* also fully restored the DNA-damage-induced electrophoretic mobility shift of Dun1 (Figure 5A).

We next tested whether these effects on Dun1 kinase activity are relevant for physiological signaling outcomes. *DUN1* has a specific DNA-damage-response function downstream of *RAD53* in the transcriptional induction of ribonucleotide reductase (RNR) subunits (Bashkirov et al., 2003; Hammet et al., 2000; Lee et al., 2003b). Consistent with the Dun1 kinase assays, *RNR3* induction under the same conditions was reduced to *DUN1*-independent (*dun1Δ*-like) levels in the *rad53Δ*, *rad53-4AQ* strain and only modestly improved in the *rad53-T5-3AQ* and *rad53-T8-3AQ* strains but restored to near WT levels in the *rad53-T5-T8-2AQ* strain, and this restoration was reversed by *DUN1* deletion (Figure 5D). In contrast to the transcriptional response, DNA-damage survival under the conditions used here is *DUN1* independent (Figure 5E, note that *dun1Δ* survival rates are similar to that of the WT). Whereas the *rad53-4AQ* strain was almost as MMS hypersensitive as the *rad53Δ* strain, this defect was substantially improved to near or identical to WT levels in any of the *rad53-T5-3AQ*, *rad53-T8-3AQ*, and *rad53-T5-T8-2AQ* strains. Similar results were also obtained in response to the replication blocking agent hydroxyurea (HU), where any single threonine in the Rad53 SCD1 was fully sufficient to maintain *RAD53*-dependent cell viability but only the simultaneous presence of two threonines was able to maintain *DUN1*-dependent *RNR3* induction (Figure S4).

The biological analyses that two adjacent phosphorylatable threonine residues in the Rad53-SCD1 are specifically required for Dun1 activation in vivo support the biochemical and structural analyses that the SCD1 has to be phosphorylated on two adjacent threonine residues (specifically, pThr5 and pThr8) for efficient binding to the Dun1-FHA. To support that these results are not merely coincidental, we introduced corresponding mutations into the two separate pThr-binding sites of the Dun1-FHA for plasmid complementation assays in a *dun1Δ* strain. Figures 5F and 5G show that both the electrophoretic mobility shift of Dun1 and its kinase activation in response to MMS treatment were dramatically reduced when the critical residues Arg60 of the first pThr-binding site or Lys100/Arg102 of the second pThr-binding site were substituted by Ala. Therefore, the *dun1-R60A* mutation phenocopies the corresponding *rad53-T8-3AQ* allele, and *dun1-K100A-R102A* mimics the *rad53-T5-3AQ* allele, demonstrating that the same phosphorylation sites and pThr-binding site residues required for Rad53-SCD1/Dun1-FHA interaction identified in biochemical and NMR analyses in vitro are just as important for Rad53-dependent Dun1 activation and signaling in vivo.

Increased Rad53-SCD1 Diphosphorylation after DNA Damage In Vivo

In order to verify that Thr5 and Thr8 of SCD1 can be simultaneously phosphorylated in vivo following DNA damage, we used the sensitive linear quadrupole ion trap Fourier transform ion cyclotron resonance (LTQ-FT) mass spectrometer to examine the phosphorylation status of Rad53. It should be noted that phosphorylation of Thr5 and Thr8 was not detected in

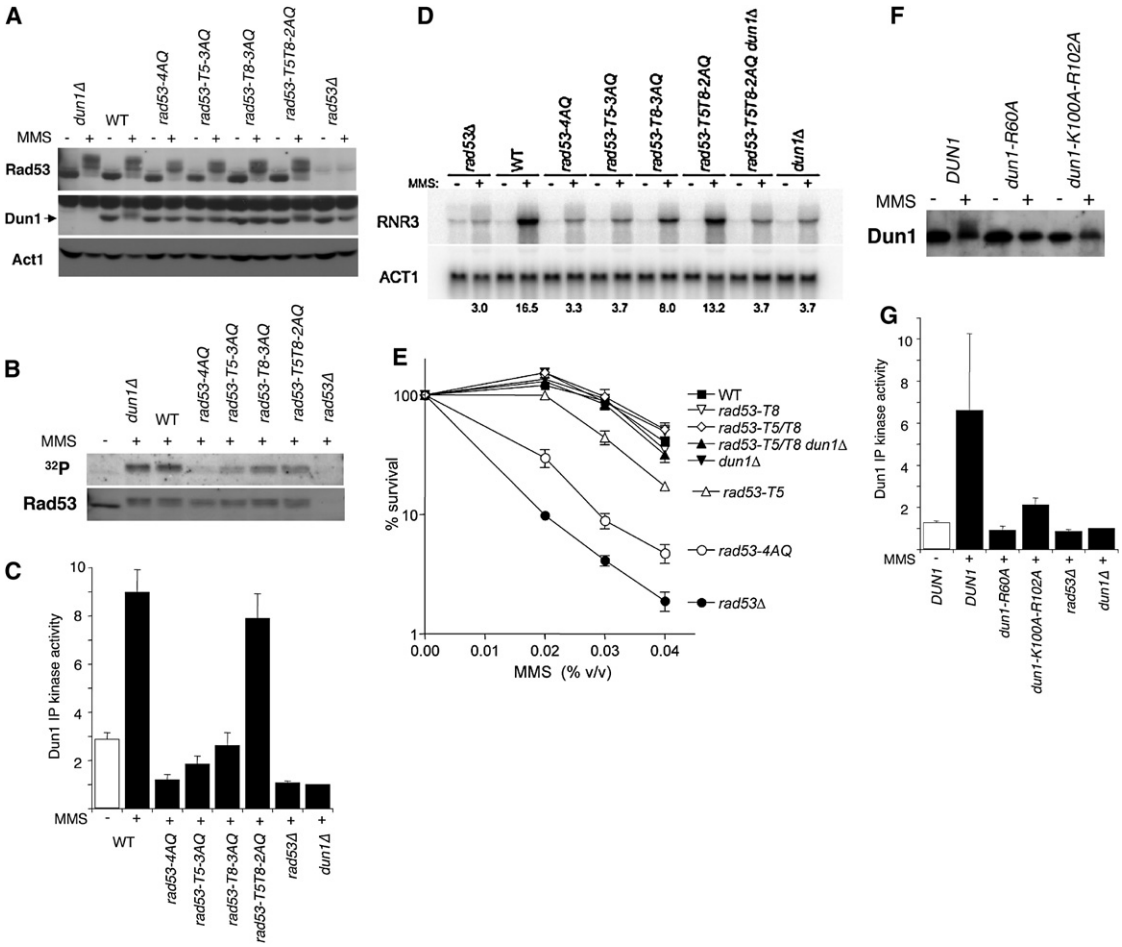

Figure 5. Differential Roles of Rad53-SCD1 Threonine Residues for Rad53 and Dun1 Functions

Unless specified, +/− signs indicate with/without 1 hr treatment using 0.05% MMS.

(A) Western blot analysis of the indicated strains using Rad53, Dun1, and Act1 antibodies.

(B) Rad53 in situ autokinase assay using γ-^{32}P-ATP (upper) and loading control blot (lower) of the indicated strains.

(C) Dun1 IP kinase assay in the indicated strains toward a synthetic peptide.

(D) Northern blot analysis of *RNR3* and *ACT1* mRNA levels in the indicated strains. Numbers indicate *RNR3*/*ACT1* ratios relative to untreated WT.

(E) DNA-damage survival assay. Strains were treated with the indicated doses of MMS for 3 hr and plated on yeast peptone dextrose medium. Survival rates are the fraction of colonies formed relative to the untreated control.

(F) Dun1 IP western blot of a *dun1Δ* strain containing the indicated *DUN1* alleles expressed from its own promoter on a centromeric plasmid.

(G) Dun1 IP kinase assays of the indicated alleles expressed from a centromeric plasmid as in (F). *dun1Δ* indicates empty pRS414 plasmid, and *rad53Δ* indicates pRS414-*DUN1* expressed in a *rad53Δdun1Δ* strain. The error bars in all quantitative data in (C), (E), and (G) are standard errors of mean from three to four independent experiments.

response to DNA damage in vivo in the two previous Rad53 phosphorylation studies (Smolka et al., 2005; Sweeney et al., 2005). After processing with titanium dioxide (TiO_2), which has better salt and detergent tolerance than immobilized metal affinity chromatography (IMAC) and has high capacity for phosphopeptide enrichment (Jensen and Larsen, 2007; Larsen et al., 2005), we were able to detect not only pT5 monophosphorylated and pT8 monophosphorylated Rad53-SCD1 (Figures S5A and S5B; also independently detected in another recent study [T. Schleker and S.M. Gasser, personal communication]) but also the pThr5-pThr8 diphosphorylated Rad53-SCD1 (Figure 6A). The results from a semiquantitative calculation suggest that the diphosphorylation of pThr5-pThr8 on Rad53-SCD1 was ~50-fold increased in response to MMS-induced DNA damage. Interestingly, pThr5-pThr8 diphosphorylation was further increased in a strain expressing kinase-dead Rad53-K227A-D339A (Figure 6B), indicating that it responds dynamically to increased checkpoint feedback when Rad53 effector functions are blocked.

The findings that SCD1 monophosphorylation is sufficient for Rad53 activation but SCD1 diphosphorylation is necessary for Dun1 activation imply that Dun1 should have a higher activation threshold than Rad53. To test this, we monitored electrophoretic mobility shifts of the two kinases as a surrogate marker for their phosphorylation-dependent activation (Figure 6C). Whereas Rad53 was near-maximally shifted after 1 hr treatment with

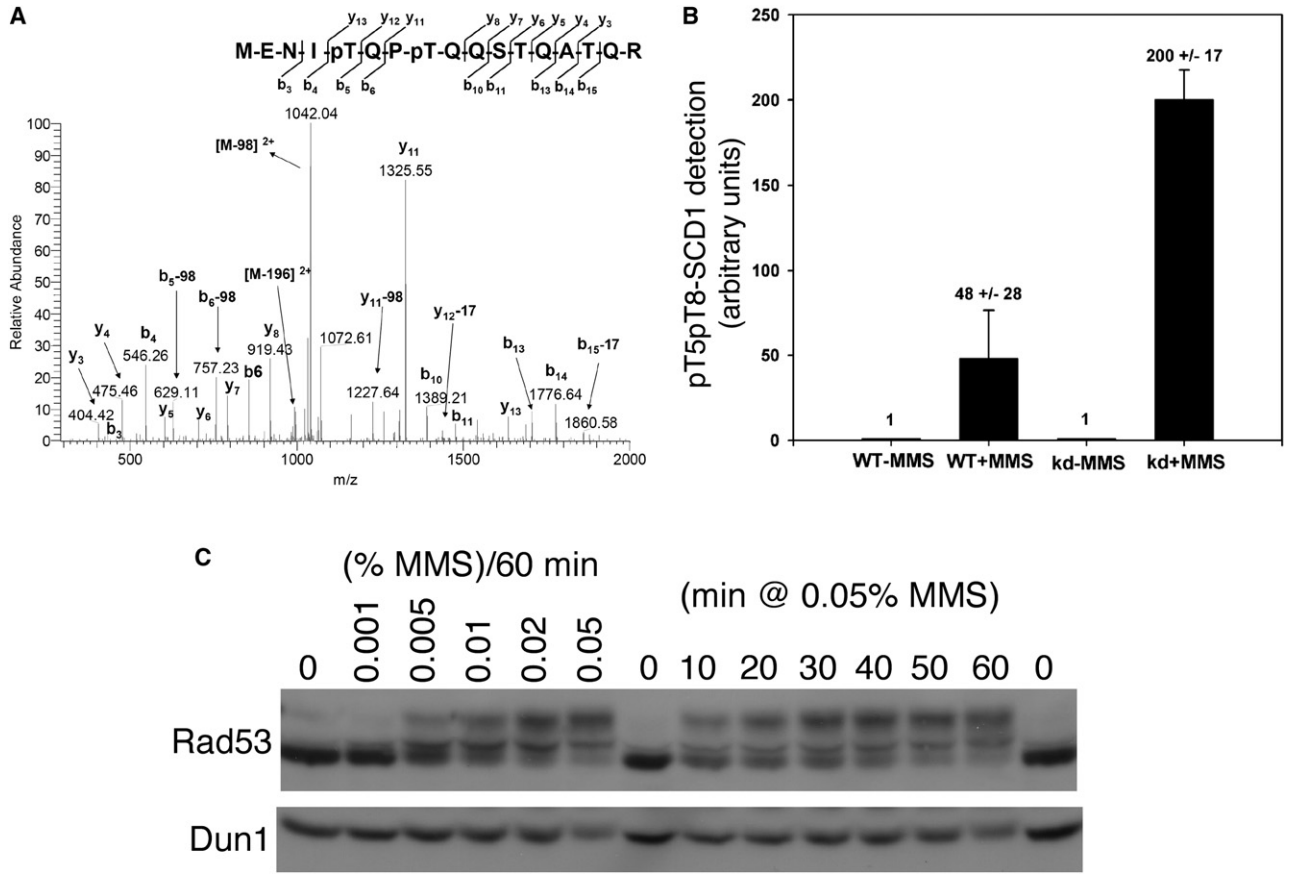

Figure 6. Rad53-SCD1 Diphosphorylation and Differential Rad53-Dun1 Activation In Vivo

(A) Tandem mass spectra of pT5-pT8 diphosphorylated Rad53-SCD1 (the N-terminal Met was N-acetylated and S-oxidized in the precursor m/z of 1090.46). The signature loss of phosphoric acid (−98) is labeled in these b and y ion assignments.

(B) Increased detection of pT5-pT8 diphosphorylated Rad53-SCD1 in WT and kinase-dead (kd) Rad53 upon MMS-induced DNA damage in vivo. The error bars indicate standard errors of mean from two independent experiments.

(C) Western blot analysis of Rad53 and Dun1 mobility shifts in WT cells in response to treatment with increasing doses of MMS for 1 hr (left part) or in 10 min intervals after addition of 0.05% MMS (right part). 0, untreated samples.

0.01% MMS, Dun1 was shifted to a slightly slower mobility band only in response to 0.05% MMS. Likewise, whereas Rad53 was rapidly shifted within 10 min at the high MMS dose, clear Dun1 shifts became apparent only after 1 hr (Figure 6C).

DISCUSSION

The main finding of this study is that the Dun1-FHA domain differs from other known FHA domains by its unprecedented binding specificity for double-pThr-containing peptides (Figure 1B). This unique binding specificity is due to a second pThr-binding site, mainly contributed by Arg102/Lys100, in the Dun1-FHA that in a way copies the "proven" design element of a basic side-chain interaction of the conserved Arg with the phosphate group of the ligand as observed in the single pThr-binding sites of other FHA domains (Figures 1D and 4). Remarkably, this second phosphopeptide-binding site of the Dun1-FHA domain is as highly pThr specific (Figure 1C) as the canonical pThr-binding site in FHA domains. The double-pThr specificity of the Dun1-FHA thus illustrates the broad range of tricks a small modular FHA domain can play, in addition to the "pT+3 rule" for a number of FHA domains (Byeon et al., 2001; Durocher et al., 2000; Li et al., 2002; Wang et al., 2000; Yuan et al., 2001), and "pT plus an extended binding surface" for Ki67-FHA (Byeon et al., 2005) (Figure 7A).

Interestingly, in addition to the Dun1-FHA domain, the same Rad53-SCD1 phosphopeptides can also bind to the Rad53-FHA1 domain, although in this case multisite phosphorylation does not improve binding affinity relative to the monophosphorylated peptides (Figure 1B). Another important finding of our study is that the SCD1 can adopt rather different conformations when bound to different proteins (compare Figures 4A and 4B). Due to low sequence complexity, SCDs are prone to be intrinsically disordered (Liao et al., 2000; Traven and Heierhorst, 2005), a property that is believed to favor accessibility for posttranslational modifications as well as increased plasticity to adopt "induced" folds that fit distinct binding partners (Dyson and Wright, 2002). The two FHA-SCD1 complexes solved here represent the first

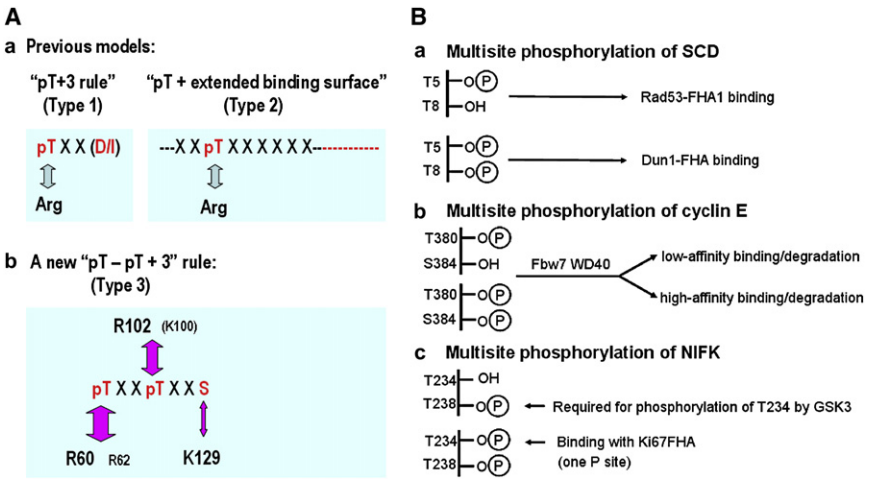

Figure 7. Comparison of the Dun1-FHA Domain Di-pThr Specificity with Other Phospho-Specific Domain Interactions

(A) Schematic illustration of the ligand specificity of FHA domains. Type 1 is the pT+3 rule from previous studies (Byeon et al., 2001; Durocher et al., 2000; Li et al., 2002; Liao et al., 2000); type 2 involves an extended binding surface, as in the case of Ki67-FHA (Byeon et al., 2005); and type 3 is represented by Dun1-FHA, which can be considered a "pT-pT+3 rule."

(B) Schematic illustration of different signaling mechanisms involving adjacent single or double site phosphorylation.

example in which the principle that the same SCD can adopt different conformations, depending on which protein it is bound to, has been directly demonstrated at the structural level.

The Dun1 residues corresponding to the conserved pThr-binding residues of Rad53 FHA1 (Arg70, Ser85, and Asn86) are Arg60, Ser74, and Thr75, respectively. Our NMR studies indicate that the two key residues Arg60 and Ser74 are recruited to different pThr-binding sites in Dun1, where they are assisted by other nonconserved residues (Arg62 assisting Arg60 in the first site and Arg102 assisting Ser74 in the second site). In addition, the two FHA domains use different sets of nonconserved residues for recognition of the "+3 site"—Rad53-FHA1 uses Arg83 (corresponding to Asp72 in Dun1) to bind the +3 Asp (Yongkiettrakul et al., 2004), while Lys129 in the Dun1-FHA β10-β11 loop (corresponding to Val136 in Rad53) contributes to the interaction by binding to Ser11 of Rad53. Taking into consideration the known structures of other FHA domain complexes, such as the Ki67-FHA complex with a 45-residue fragment of NIFK (Byeon et al., 2005), one can conclude that different FHA domains use very different binding mechanisms to confer their binding specificity beyond the common pThr requirement. The versatility of FHA domains in ligand recognition and biological functions is further evidenced by our recent finding that the same FHA domain, Rad53 FHA1, can bind either pTXXD or pTXXI ligand, with different sets of residues (Mahajan et al., 2005).

Given the diversity and versatility of FHA domains, it remains to be determined if the dual-pThr specificity observed for Dun1 FHA also exists in other FHA domains. Interestingly, analysis of 2044 FHA sequence alignments generated by the Pfam server suggested that this property may be more widespread. Figure S6 lists several other FHA domains, mostly from bacterial species, that contain an Arg residue corresponding in position to the critical Dun1-Arg102 of the second pThr-binding site. Whereas this Arg seems to occur as an exception in Chk2 and Nbs1 in some invertebrates (e.g., *Drosophila* and *C. elegans*) but not in all other species, it seems highly conserved in microspherulin and the Fkh2 transcription factor. For the FHA domain of yeast Fkh2, it is interesting to note that the bona fide Fkh2-FHA domain ligand Ndd1 requires Cdc28/Clb-dependent phosphorylation for this interaction and that Ndd1 contains two very closely spaced threonine-containing Cdc28/Clb phosphorylation sites at positions 179 and 183 (TPAKTPLR). Although phosphorylation of Ndd1 Thr319 has been shown to be important for its interaction with Fkh2, Ndd1-Fkh2 interactions are regulated in a complex manner throughout the cell cycle (Pic-Taylor et al., 2004; Reynolds et al., 2003). It may thus be speculated that Ndd1-pT179-pT183 diphosphorylation may facilitate Fkh2-FHA binding under certain conditions.

Activation of FHA domain-containing kinases is widely believed to be a two-step process that involves their initial phosphorylation by an ATM/ATR-like kinase that triggers oligomerization-dependent multisite autophosphorylation. In the human Chk2 kinase and fission yeast Cds1, kinase activation involves intermolecular interactions between the phosphorylated N-terminal SCD and the single N-terminal FHA domains (Ahn et al., 2002; Tanaka et al., 2001). Although we have shown here that the Rad53-SCD1 can interact with the Rad53-FHA1 in a similar pThr-dependent manner (Figures 1 and 4), it should be stressed that, in contrast to the SCD1, the Rad53-FHA1 domain overall seems to play only a minor role in Rad53 activation compared to the Rad53-FHA2 domain (Pike et al., 2003; Schwartz et al., 2003; Sweeney et al., 2005), except in G2/M-arrested cells (Pike et al., 2003, 2004). However, it is unlikely that the FHA2 fulfils its important role in Rad53 activation as an intermolecular SCD1-pThr-binding domain, as we failed to detect appreciable binding between the isolated FHA2 (that bound other peptides under these conditions perfectly well) and SCD1-derived phosphopeptides in SPR analyses. Therefore, although our results with integrated *rad53* alleles (Figure 5) confirm the importance of SCD1 phosphorylation for Rad53 activation revealed by previous in vivo plasmid complementation assays (Lee et al., 2003b) and in vitro kinase assays (Chen et al., 2007), it appears that the SCD1 may have other yet-to-be-deciphered FHA domain-independent functions in Rad53 activation.

The finding that double phosphorylation increases the affinity of the SCD1 for the Dun1-FHA domain is generally reminiscent of the mechanism of how multisite phosphorylation of Sic1 (Nash et al., 2001) or cyclin E (Hao et al., 2007) increases their binding to ubiquitin ligases (Figure 7B). However, in the case of the Rad53-SCD1, the phosphorylation state may add another

layer of complexity, considering that the monophosphorylated SCD1 has ~10-fold higher affinity for the Rad53-FHA1 than Dun1-FHA domain, whereas multiphosphorylated SCD1 has ~10-fold higher affinity for the Dun1-FHA than Rad53-FHA1 domain (Figure 1B). Thus, the phospho-counting mechanism reported here is unprecedented in that it involves the SQ/TQ cluster and that it regulates different signaling outcomes (Figure 7B). It also differs from the example of NIFK binding to the Ki67-FHA, where multisite phosphorylation is a sequential process in which the first site serves to recruit another kinase to phosphorylate the actual binding site (Byeon et al., 2005) (Figure 7B).

Considering that SCD1 monophosphorylation seems sufficient for Rad53 activation but Dun1 activation seems to require multisite phosphorylation of the same region, it is tempting to speculate that the phosphorylation state of the Rad53-SCD1 may provide a molecular mechanism for the higher threshold for Dun1 activation than Rad53 activation in response to DNA damage (Figure 6C). This graded response could explain how the same SCD might regulate the sequential activation of two members of a kinase cascade in a temporally ordered manner and would be consistent with the notions that Rad53 is overall more important than Dun1 for cell survival in response to DNA damage (Figure 5 and Figure S4) as well as cell viability under basal conditions (unless *rad53Δ* cells are maintained by extragenic lethality suppressors such as *sml1Δ* used here [Zhao and Rothstein, 2002]).

Finally, it has recently been shown that numerous human proteins can be simultaneously phosphorylated on multiple adjacent SQ/TQ motifs in response to DNA damage (Matsuoka et al., 2007). Although it remains to be determined if other FHAs share the multiphospho-site specificity of the Dun1 FHA domain, the phospho-counting mechanism presented here may provide one structural paradigm that could be helpful to understand how multisite phosphorylation of SCDs contributes to the diversified cellular response to DNA damage.

EXPERIMENTAL PROCEDURES

Expression and Purification of Dun1-FHA and Rad53-FHA1

The gene encoding Dun1-FHA (residues 19–159) with a His-tag at the C terminus was cloned into pQE60 vector (Hammet et al., 2000), and it was used as template for generating seven mutants by site-directed mutagenesis. All mutants were then cloned into pET101/D-TOPO vector in order to have better overexpression. Nonlabeled, [*U*-^{15}N]-, [*U*-^{13}C, ^{15}N]-, and [*U*-^{13}C, ^{15}N, 70% ^{2}H]-labeled WT and mutant Dun1-FHA (19–159) were overexpressed in *E. coli* with 0.5 mM IPTG. Cells were lysed either by sonication or by a microfluidizer in buffer consisting of 50 mM Na_2HPO_4 (pH 7.5), 500 mM NaCl, 5 mM β-mercaptoethanol, 0.5% Triton X-100, 1 tablet of protease inhibitor cocktail (Roche), and 1 mg/mL lysozyme from chicken egg white. The protein was purified using Ni-NTA agarose (QIAGEN), SP-sepharose ion-exchange column, and S-100 gel filtration chromatography. Rad53-FHA1 was expressed and purified as described (Liao et al., 2000).

The Dissociation Equilibrium Constant Determination by SPR

All peptides were biotinylated by incubating with EZ-Link Sulfo-NHS-Biotin (Pierce) in 5 mM Na_2HPO_4 buffer for 2 hr at room temperature. All biotinylated peptide solutions were diluted to 50 μM with commercial HBS-EP buffer (10 mM HEPES, 150 mM NaCl, 3 mM EDTA, and 0.005% Tween-20 [pH 7.4]) followed by immobilization at each channel with 20 μL/min flow rate for 2 min on sensor chip SA. A blank channel without any immobilization was used as a control. Protein solutions with a series of increasing concentration (0.01–200 μM) were applied to all four channels at 25 μL/min flow rate for 180 s of dissociation time. At least seven different concentrations of protein were investigated for each protein-peptide-binding interaction. SigmaPlot was used to fit the data to a single rectangular hyperbolic curve to extract K_D. The hyperbola function shown below was used to plot maximal responses and corresponding concentration: $y = RU_{max}x/(K_D + c)$, where y indicates the response in response unit (RU), RU_{max} is the maximum response, and x is the protein concentration.

Structural Studies on Dun1-FHA/pT5pT8 and Rad53-FHA1/pT5 Complexes

The solution structure of free Dun1 was determined as described previously for other FHA domains (Li et al., 2004; Liao et al., 2000) and described in Supplemental Data. In the determination of the structures of complexes, aliquots of stock peptide solution were added to the protein solution while being monitored by 2D ^{1}H-^{15}N HSQC on the [*U*-^{13}C, ^{15}N]-labeled Dun1-FHA. This was followed by isotope-filtered experiments, including 2D ^{13}C/^{15}N-filtered NOESY, TOCSY, and COSY; 3D ^{13}C/^{15}N-filtered (*f*1); ^{13}C-edited (*f*3) NOESY; and 3D ^{13}C-edited (*f*1), ^{13}C/^{15}N-filtered (*f*3) NOESY (Breeze, 2000). 3D ^{13}C-edited NOESY and 3D ^{15}N-edited NOESY were collected with 150 ms mixing time to aid intermolecular NOE assignments as well as to evaluate the conformational changes of Dun1-FHA in complex with the pT-peptide. HNCA and HN(CO)CA were also recorded to resolve ambiguities in backbone sequential assignment. The structure was generated using CNS software with simulated annealing protocol.

Yeast Experiments

Yeast experiments were performed in the W303-1A *RAD5 sml1Δ* background. *rad53* mutations were integrated into the endogenous gene locus. *dun1* mutations were assessed by plasmid complementation. Antibodies for blots and IP were directed against native untagged Rad53, Dun1, and Act1. For DNA-damage sensitivity assays, cells were treated in solution and replated on drug-free medium to determine colony formation relative to untreated colonies. Rad53 kinase activity was measured in in situ autophosphorylation assays, Dun1 kinase activity was measured in IP kinase assays against a synthetic peptide, and northern blots were performed by using ^{32}P-labeled cDNA probes and quantified by phosphoimaging (Pike et al., 2003). For mass spectrometry, kinase-dead *rad53-K227A-D339A* was cloned into pYES2/CT and expressed in a *rad53Δdun1Δ* strain, followed by MMS treatment, purification using anti-V5 agarose, and SDS-PAGE. Peptide nanoflow LC-MS/MS experiments were performed on a LTQ-FT mass spectrometer (Thermo Electron) as described in the Supplemental Data.

ACCESSION NUMBERS

Coordinates of the Dun1-FHA, Dun1-FHA/pT5pT8, and Rad53-FHA/pT5 (20 conformers each) have been deposited in the Protein Data Bank under ID codes 2JQJ, 2JQL, and 2JQI, respectively.

SUPPLEMENTAL DATA

The Supplemental Data include Supplemental Experimental Procedures, six figures, two tables, and Supplemental References and can be found with this article online at http://www.molecule.org/cgi/content/full/30/6/767/DC1/.

ACKNOWLEDGMENTS

We thank Hui-Ming Yu for syntheses of phosphopeptides; Chi-Fon Chang, Fu-Yang Lin, and Wen-Jin Wu for assisting NMR experiments; Nora Tenis for assistance with cloning and blot analysis; David Stern for the original pRS316-*RAD53* plasmid; Susan Gasser for sharing unpublished data; Brietta Pike, Bruce Kemp, Bostjan Kobe, Colin House, Trazel Teh, Paul Gooley, Helen Blanchard, Marcos Fontes, and the late Ken Mitchelhill for earlier analyses of the Dun1-FHA domain; and Hsiu-Chien Chan for help in preparing Figure 4. Supported by research grants from National Health Research Institute (NHRI)

(EX95-9508NI) of Taiwan, the National Institutes of Health (NIH) (CA69472) of USA, and Genomics Research Institute (GRC) of Taiwan to M.-D.T.; Australian National Health and Medical Research Council (NHMRC) project grants and NHMRC Senior Research Fellowship to J.H.; and NHMRC C.J. Martin Fellowship to A.H. NMR was performed at the NRPGM NMR Core of Taiwan and the Campus Chemical Instrument Center of The Ohio State University (CCIC of OSU). H.L. discovered the preference of Dun1-FHA for diphosphorylated SCD1 and performed other biochemical experiments. C.Y. solved the NMR structures and uncovered the structural basis of phosphocounting. A.H. and J.H. designed, performed, and interpreted the biological experiments. H.L., A.M., M.-R.W., and M.-I.S. performed some NMR and SPR, and E.S.-W.C. performed MS experiments. M.-D.T. coordinated and led the project. H.L., C.Y., J.H., and M.-D.T. wrote the paper. The authors declare no competing financial interests.

Received: February 11, 2008
Revised: March 21, 2008
Accepted: May 13, 2008
Published: June 19, 2008

REFERENCES

Ahn, J.Y., Li, X., Davis, H.L., and Canman, C.E. (2002). Phosphorylation of threonine 68 promotes oligomerization and autophosphorylation of the Chk2 protein kinase via the forkhead-associated domain. J. Biol. Chem. *277*, 19389–19395.

Bashkirov, V.I., Bashkirova, E.V., Haghnazari, E., and Heyer, W.D. (2003). Direct kinase-to-kinase signaling mediated by the FHA phosphoprotein recognition domain of the Dun1 DNA damage checkpoint kinase. Mol. Cell. Biol. *23*, 1441–1452.

Breeze, A.L. (2000). Isotope-filtered NMR methods for the study of biomolecular structure and interactions. Prog. Nucl. Magn. Reson. Spectrosc. *36*, 323–372.

Byeon, I.J., Yongkiettrakul, S., and Tsai, M.D. (2001). Solution structure of the yeast Rad53 FHA2 complexed with a phosphothreonine peptide pTXXL: comparison with the structures of FHA2-pYXL and FHA1-pTXXD complexes. J. Mol. Biol. *314*, 577–588.

Byeon, I.J., Li, H., Song, H., Gronenborn, A.M., and Tsai, M.D. (2005). Sequential phosphorylation and multisite interactions characterize specific target recognition by the FHA domain of Ki67. Nat. Struct. Mol. Biol. *12*, 987–993.

Chen, S.H., Smolka, M.B., and Zhou, H. (2007). Mechanism of Dun1 activation by Rad53 phosphorylation in Saccharomyces cerevisiae. J. Biol. Chem. *282*, 986–995.

Durocher, D., and Jackson, S.P. (2002). The FHA domain. FEBS Lett. *513*, 58–66.

Durocher, D., Taylor, I.A., Sarbassova, D., Haire, L.F., Westcott, S.L., Jackson, S.P., Smerdon, S.J., and Yaffe, M.B. (2000). The molecular basis of FHA domain:phosphopeptide binding specificity and implications for phospho-dependent signaling mechanisms. Mol. Cell *6*, 1169–1182.

Dyson, H.J., and Wright, P.E. (2002). Coupling of folding and binding for unstructured proteins. Curr. Opin. Struct. Biol. *12*, 54–60.

Gardner, R., Putnam, C.W., and Weinert, T. (1999). RAD53, DUN1 and PDS1 define two parallel G2/M checkpoint pathways in budding yeast. EMBO J. *18*, 3173–3185.

Hammet, A., Pike, B.L., Mitchelhill, K.I., Teh, T., Kobe, B., House, C.M., Kemp, B.E., and Heierhorst, J. (2000). FHA domain boundaries of the dun1p and rad53p cell cycle checkpoint kinases. FEBS Lett. *471*, 141–146.

Hammet, A., Pike, B.L., and Heierhorst, J. (2002). Posttranscriptional regulation of the RAD5 DNA repair gene by the Dun1 kinase and the Pan2-Pan3 poly(A)-nuclease complex contributes to survival of replication blocks. J. Biol. Chem. *277*, 22469–22474.

Hao, B., Oehlmann, S., Sowa, M.E., Harper, J.W., and Pavletich, N.P. (2007). Structure of a Fbw7-Skp1-cyclin E complex: multisite-phosphorylated substrate recognition by SCF ubiquitin ligases. Mol. Cell *26*, 131–143.

Jensen, S.S., and Larsen, M.R. (2007). Evaluation of the impact of some experimental procedures on different phosphopeptide enrichment techniques. Rapid Commun. Mass Spectrom. *21*, 3635–3645.

Kim, H., Chen, J., and Yu, X. (2007). Ubiquitin-binding protein RAP80 mediates BRCA1-dependent DNA damage response. Science *316*, 1202–1205.

Kolas, N.K., Chapman, J.R., Nakada, S., Ylanko, J., Chahwan, R., Sweeney, F.D., Panier, S., Mendez, M., Wildenhain, J., Thomson, T.M., et al. (2007). Orchestration of the DNA-damage response by the RNF8 ubiquitin ligase. Science *318*, 1637–1640.

Larsen, M.R., Thingholm, T.E., Jensen, O.N., Roepstorff, P., and Jorgensen, T.J. (2005). Highly selective enrichment of phosphorylated peptides from peptide mixtures using titanium dioxide microcolumns. Mol. Cell. Proteomics *4*, 873–886.

Lee, G.I., Ding, Z., Walker, J.C., and Van Doren, S.R. (2003a). NMR structure of the forkhead-associated domain from the Arabidopsis receptor kinase-associated protein phosphatase. Proc. Natl. Acad. Sci. USA *100*, 11261–11266.

Lee, S.J., Schwartz, M.F., Duong, J.K., and Stern, D.F. (2003b). Rad53 phosphorylation site clusters are important for Rad53 regulation and signaling. Mol. Cell. Biol. *23*, 6300–6314.

Li, J., Williams, B.L., Haire, L.F., Goldberg, M., Wilker, E., Durocher, D., Yaffe, M.B., Jackson, S.P., and Smerdon, S.J. (2002). Structural and functional versatility of the FHA domain in DNA-damage signaling by the tumor suppressor kinase Chk2. Mol. Cell *9*, 1045–1054.

Li, H., Byeon, I.J., Ju, Y., and Tsai, M.D. (2004). Structure of human Ki67 FHA domain and its binding to a phosphoprotein fragment from hNIFK reveal unique recognition sites and new views to the structural basis of FHA domain functions. J. Mol. Biol. *335*, 371–381.

Liao, H., Byeon, I.J., and Tsai, M.D. (1999). Structure and function of a new phosphopeptide-binding domain containing the FHA2 of Rad53. J. Mol. Biol. *294*, 1041–1049.

Liao, H., Yuan, C., Su, M.I., Yongkiettrakul, S., Qin, D., Li, H., Byeon, I.J., Pei, D., and Tsai, M.D. (2000). Structure of the FHA1 domain of yeast Rad53 and identification of binding sites for both FHA1 and its target protein Rad9. J. Mol. Biol. *304*, 941–951.

Lopes, M., Cotta-Ramusino, C., Pellicioli, A., Liberi, G., Plevani, P., Muzi-Falconi, M., Newlon, C.S., and Foiani, M. (2001). The DNA replication checkpoint response stabilizes stalled replication forks. Nature *412*, 557–561.

Mahajan, A., Yuan, C., Pike, B.L., Heierhorst, J., Chang, C.F., and Tsai, M.D. (2005). FHA domain-ligand interactions: importance of integrating chemical and biological approaches. J. Am. Chem. Soc. *127*, 14572–14573.

Manke, I.A., Lowery, D.M., Nguyen, A., and Yaffe, M.B. (2003). BRCT repeats as phosphopeptide-binding modules involved in protein targeting. Science *302*, 636–639.

Matsuoka, S., Huang, M., and Elledge, S.J. (1998). Linkage of ATM to cell cycle regulation by the Chk2 protein kinase. Science *282*, 1893–1897.

Matsuoka, S., Ballif, B.A., Smogorzewska, A., McDonald, E.R., 3rd, Hurov, K.E., Luo, J., Bakalarski, C.E., Zhao, Z., Solimini, N., Lerenthal, Y., et al. (2007). ATM and ATR substrate analysis reveals extensive protein networks responsive to DNA damage. Science *316*, 1160–1166.

Myung, K., Datta, A., and Kolodner, R.D. (2001). Suppression of spontaneous chromosomal rearrangements by S phase checkpoint functions in Saccharomyces cerevisiae. Cell *104*, 397–408.

Nash, P., Tang, X., Orlicky, S., Chen, Q., Gertler, F.B., Mendenhall, M.D., Sicheri, F., Pawson, T., and Tyers, M. (2001). Multisite phosphorylation of a CDK inhibitor sets a threshold for the onset of DNA replication. Nature *414*, 514–521.

Pic-Taylor, A., Darieva, Z., Morgan, B.A., and Sharrocks, A.D. (2004). Regulation of cell cycle-specific gene expression through cyclin-dependent kinase-mediated phosphorylation of the forkhead transcription factor Fkh2p. Mol. Cell. Biol. *24*, 10036–10046.

Pike, B.L., Yongkiettrakul, S., Tsai, M.D., and Heierhorst, J. (2003). Diverse but overlapping functions of the two forkhead-associated (FHA) domains in Rad53 checkpoint kinase activation. J. Biol. Chem. *278*, 30421–30424.

Pike, B.L., Tenis, N., and Heierhorst, J. (2004). Rad53 kinase activation-independent replication checkpoint function of the N-terminal forkhead-associated (FHA1) domain. J. Biol. Chem. *279*, 39636–39644.

Reynolds, D., Shi, B.J., McLean, C., Katsis, F., Kemp, B., and Dalton, S. (2003). Recruitment of Thr 319-phosphorylated Ndd1p to the FHA domain of Fkh2p requires Clb kinase activity: a mechanism for CLB cluster gene activation. Genes Dev. *17*, 1789–1802.

Sanchez, Y., Desany, B.A., Jones, W.J., Liu, Q., Wang, B., and Elledge, S.J. (1996). Regulation of RAD53 by the ATM-like kinases MEC1 and TEL1 in yeast cell cycle checkpoint pathways. Science *271*, 357–360.

Schwartz, M.F., Lee, S.J., Duong, J.K., Eminaga, S., and Stern, D.F. (2003). FHA domain-mediated DNA checkpoint regulation of Rad53. Cell Cycle *2*, 384–396.

Smolka, M.B., Albuquerque, C.P., Chen, S.H., Schmidt, K.H., Wei, X.X., Kolodner, R.D., and Zhou, H. (2005). Dynamic changes in protein-protein interaction and protein phosphorylation probed with amine-reactive isotope tag. Mol. Cell. Proteomics *4*, 1358–1369.

Stavridi, E.S., Huyen, Y., Loreto, I.R., Scolnick, D.M., Halazonetis, T.D., Pavletich, N.P., and Jeffrey, P.D. (2002). Crystal structure of the FHA domain of the Chfr mitotic checkpoint protein and its complex with tungstate. Structure *10*, 891–899.

Stokes, M.P., Rush, J., Macneill, J., Ren, J.M., Sprott, K., Nardone, J., Yang, V., Beausoleil, S.A., Gygi, S.P., Livingstone, M., et al. (2007). Profiling of UV-induced ATM/ATR signaling pathways. Proc. Natl. Acad. Sci. USA *104*, 19855–19860.

Sun, Z., Hsiao, J., Fay, D.S., and Stern, D.F. (1998). Rad53 FHA domain associated with phosphorylated Rad9 in the DNA damage checkpoint. Science *281*, 272–274.

Sweeney, F.D., Yang, F., Chi, A., Shabanowitz, J., Hunt, D.F., and Durocher, D. (2005). Saccharomyces cerevisiae Rad9 acts as a Mec1 adaptor to allow Rad53 activation. Curr. Biol. *15*, 1364–1375.

Tanaka, K., Boddy, M.N., Chen, X.B., McGowan, C.H., and Russell, P. (2001). Threonine-11, phosphorylated by Rad3 and atm in vitro, is required for activation of fission yeast checkpoint kinase Cds1. Mol. Cell. Biol. *21*, 3398–3404.

Tercero, J.A., and Diffley, J.F. (2001). Regulation of DNA replication fork progression through damaged DNA by the Mec1/Rad53 checkpoint. Nature *412*, 553–557.

Traven, A., and Heierhorst, J. (2005). SQ/TQ cluster domains: concentrated ATM/ATR kinase phosphorylation site regions in DNA-damage-response proteins. Bioessays *27*, 397–407.

Wang, P., Byeon, I.J., Liao, H., Beebe, K.D., Yongkiettrakul, S., Pei, D., and Tsai, M.D. (2000). II. Structure and specificity of the interaction between the FHA2 domain of Rad53 and phosphotyrosyl peptides. J. Mol. Biol. *302*, 927–940.

Yongkiettrakul, S., Byeon, I.J., and Tsai, M.D. (2004). The ligand specificity of yeast Rad53 FHA domains at the +3 position is determined by nonconserved residues. Biochemistry *43*, 3862–3869.

Yuan, C., Yongkiettrakul, S., Byeon, I.J., Zhou, S., and Tsai, M.D. (2001). Solution structures of two FHA1-phosphothreonine peptide complexes provide insight into the structural basis of the ligand specificity of FHA1 from yeast Rad53. J. Mol. Biol. *314*, 563–575.

Zhao, X., and Rothstein, R. (2002). The Dun1 checkpoint kinase phosphorylates and regulates the ribonucleotide reductase inhibitor Sml1. Proc. Natl. Acad. Sci. USA *99*, 3746–3751.